Electrical conductivity fluctuations as a tracer to determine time-dependent transport characteristics in hyporheic sediments

Jonas L. Schaper[1], Olaf A. Cirpka[1], Joerg Lewandowski[2,3], Cristiane Zarfl[1]

5   [1]Department of Geosciences, Eberhard Karls University of Tübingen, Tübingen, 72076, Germany
[2]Department Ecohydrology and Biogeochemistry, Leibniz-Institute of Freshwater Ecology and Inland Fisheries, Berlin, 12587, Germany
[3] Geography Department, Humboldt University Berlin, Berlin, 12489, Germany

10   *Correspondence to*: Jonas. L. Schaper (jonas.schaper@uni-tuebingen.de)

Abstract. Assessing water transport in riverbed sediments is important for quantifying the effective reactivity of hyporheic sediments and the magnitude of groundwater-surface water exchange flows. A typical approach of estimating transport in riverbed sediments is by measuring natural tracers such as heat or electrical conductivity (EC) and fitting models to them that assume time-independent travel time distributions, implying steady-state flow. Here, we use a transport parameterization that

15   is based on the advection-dispersion equation (ADE) with coefficients that continuously vary in time. The ADE is solved numerically and its solution is fitted to measured EC time series using Bayesian parameter inference. A continuous function of model parameters is constructed by smoothly interpolating between point values with different temporal resolution, and Tikhonov regularization is used to avoid spurious parameter fluctuations. The approach is tested using EC time series synchronously measured in surface water and hyporheic porewater of two urban rivers in Germany and one urban river in

20   South Australia. For all datasets the goodness of fit was improved by introducing a time-dependent EC offset. Estimated porewater velocities were highly transient in three out of the four datasets with values increasing by a factor of 6 over the course of 24 h and were likely related to both variations of hydraulic gradients along and spatial shifting of flow paths. Non-parametric deconvolution indicated that transport in three out of four datasets could be characterized as Fickian, but that flux transients may induce multimodality in stationary travel time distributions. Given the high temporal dynamics, transport

25   characteristics encountered in the streambed sediments of the three investigated urban rivers, we envision that the presented model is a valuable tool to improve the accuracy of both reactive transport simulations and assessments of biogeochemical turnover in riverbed sediments.

Plain language summary: In this study, we present a model approach to quantify river water to riverbed sediment travel times

30   as a continuous function of time using natural electrical conductivity fluctuations as a tracer. We show that apparent water travel times from surface waters through riverbed sediments can be highly dynamic, which may be caused by actual variations of porewater velocity following diurnal variations of head gradients or by a shift of the spatial arrangement of flow paths and their lengths.

1 Introduction

The hyporheic zone (HZ), i.e., the riverbed sediments where groundwater and surface waters interact, provides habitats for freshwater biota, regulates the magnitude of groundwater-surface water exchange and plays an important role for biogeochemical cycling and pollutant dynamics in lotic surface waters (Boano et al., 2014; Lewandowski et al., 2019). Quantitative assessments of groundwater-surface water exchange, biogeochemical cycling, and the fate of anthropogenic compounds in riverbeds sediments require a thorough understanding of the transport characteristics therein. Transport characteristics control the time available for reactions to occur (Frei and Peiffer, 2016; Pittroff et al., 2017; Ginn, 1999) and influence the temperature distribution and biogeochemical conditions such as and redox zonation in riverbed sediments (Zarnetske et al., 2011). Both, temperature and biogeochemistry control the microbial community structure (Peralta-Maraver et al., 2018) and the reactivity of anthropogenic compounds, nutrients and dissolved organic carbon in the sediments (Schaper et al., 2019; Harvey et al., 2013). Knowledge on transport characteristics in riverbed sediments can furthermore inform investigations on the extent and magnitude of hyporheic exchange flows (Knapp et al., 2017) and can be relevant for drinking water management when riverbank filtration is used for drinking water production (Huntscha et al., 2013; Heberer, 2002).

The distribution of travel times at sampling points in riverbed sediments is commonly assessed by fitting parametric (Luo et al., 2006; Maloszewski and Zuber, 1993) or non-parametric transfer functions (Cirpka et al., 2007; McCallum et al., 2014) to time series of artificial or natural tracers, or by adjusting the advection-dispersion equation to the data (Höhne et al., 2021; Schaper et al., 2019). Because of mixing along and between hyporheic flow paths, samples collected at idealized points within the HZ are typically characterized by a distribution of travel times rather than a single travel-time value (Varni and Carrera, 1998; Leray et al., 2016; Engdahl et al., 2016; McCallum et al., 2015; Danckwerts, 1953; McCallum et al., 2014). Artificial tracers have the advantage that background concentrations are practically zero and that tracer breakthrough curves can be unambiguously related to input signals. However, depending on river flow, large amounts of the artificial tracer might have to be injected into the surface water to detect breakthrough curves in riverbed sediments. Moreover, tracer recoveries and travel-time distributions inferred from artificial-tracer injections are valid only for the hydrological conditions encountered during the tracer test and thus fail to capture temporal variability inherent to lotic systems. Consequently, time series of natural or environmental tracers such as heat and electrical conductivity (EC) are often used to infer transport characteristics in riverbed sediments.

The applicability of EC and heat as natural tracers for riverbed sediments relies on the propagation of fluctuations of these properties from the river into the riverbed. One of the most common approaches uses diurnal temperature fluctuations as signal (Stallman, 1965; Hatch et al., 2006), which can be interpreted both for infiltrating and exfiltrating conditions. However, heat transport in sediments strongly depends on the porosity and the mineral composition of the sediments, which introduces a relatively large uncertainty in the estimate of porewater velocities from temperature records. Also, temperature signals undergo comparably strong dispersion, making diurnal variation vanish at depths beyond about 1 m (Vogt et al., 2010).

EC fluctuations in lotic surface water can be caused by natural in-stream processes such as diurnal variations of stream metabolism and associated biogeochemical cycling (de Montety et al., 2011; Hayashi et al., 2012) or time-varying mixing of waters from sources with different EC, e.g., effluents from wastewater treatment plants versus groundwater discharge (Jaeger et al., 2019). In freshwaters, the ions contributing to EC hardly sorb and thus, transport of EC signals is much less affected by retardation or other reactions than temperature signals. Also, the dispersion of the ions is practically that of an ideal tracer, rendering EC a more precise tracer to determine travel-time distributions characteristics in the riverbed sediments than heat. However, EC signals in riverbed sediments are influenced by precipitation and dissolution of minerals (particularly calcite), cation exchange, and other reactive processes so that EC is not fully conservative. EC time series in riverbed sediments and alluvial aquifers have predominately been evaluated by methods that assume transport parameters to be time-invariant such as cross-correlation (Schmidt et al., 2012; Vieweg et al., 2016; Sheets et al., 2002), non-parametric deconvolution (Cirpka et al., 2007), or numerical solutions of the advection dispersion equation (ADE) with constant coefficients (Schaper et al., 2019). A general advantage of parameterized transfer functions, such as the inverse-Gaussian distribution resulting from the ADE, is that they are fully characterized by a few parameters, which need to be estimated in model calibration. This simplicity comes at the expense that travel-time distributions (TTD) must adhere to pre-defined shapes and thus potential features of the real TTDs such as broad peaks, multi-modality and long tails might be missed. Non-parametric deconvolution, on the contrary, can estimate any shape of the TTD, but is prone to noise in the time series. They typically assume that transport characteristics are time invariant. In analogy to the approach of Keery et al. (2007), Vogt et al. (2010) used dynamic harmonic regression (Young et al., 1999) to extract the nonstationary harmonic component with the period of one day from EC time series in a river and its sediment to estimate time-dependent mean surface water to groundwater travel time from the phase shift between the two signals. However, this approach requires surface water EC fluctuations to be quasi-sinusoidal and its accuracy is largely determined by the performance of the respective signal-filtering technique. Model approaches that allow to estimate time-varying porewater velocities and dispersion coefficients from EC time series, are thus widely lacking.

Groundwater-surface water exchange flows can be can be highly dynamic as a result of flow variations in the river (Wu et al., 2020, 2018). Direct field observations of flux transients resulting from river flow variations over relatively short timescales (<24 h) are relatively scarce and the ability of EC as tracer to capture flux transients in streambed sediments has hardly been explored. It is furthermore unclear, to which extent flux transients influence the shape of TTDs in riverbed sediments and thus the accuracy of ADE based model approaches along relatively small (< 20 cm) spatial scales.

The aim of the present study therefore was to develop and test a versatile numerical modeling approach that allows determining dynamic travel-time distributions, parameterized by an apparent longitudinal dispersivity and time-varying porewater velocities, from EC time series in riverbed sediments. Because we have observed offsets in the mean EC values between the river water and the porewater in the sediment, we also estimate a time-varying systematic offset that may reflect reactive processes in the sediment.

A highly flexible model that allows time-variable transport coefficients, including a time-variable offset, is prone to misinterpretation of the data. In the most extreme case, all differences between the two EC time series would be interpreted as

Hydrology and
Earth System
Sciences
Discussions
EGU
Open Access

transport-independent offsets, whereas another extreme case would make the velocities fluctuate at very high frequencies to match every noise-related fluctuation in the data. To avoid such effects, the temporal resolution of the apparent porewater velocity and the EC offset must be chosen wisely, and smoothing of the time-varying coefficients may need to be enforced by Tikhonov regularization (Tikhonov and Arsenin, 1977). In the present study, we outline a strategy how to determine the

105 temporal resolution of coefficients and the regularization weights for given data. Subsequently, we discuss the applicability of the approach and the effects of parameter regularization schemes in light of EC time series collected in riverbed sediments (flow paths < 20 cm) of three rivers with different patterns of EC fluctuations in surface water. We then compare the estimates of the time-dependent mean travel times from the rivers to their HZs obtained by the numerical model to stationary travel-time distributions inferred by non-parametric deconvolution, testing whether features obtained by the non-parametric stationary

110 deconvolution can be related to non-stationarity of transport.

2 Materials & Methods

2.1 Data acquisition and study sites

Time series of specific electrical conductivity, total pressure, and temperature in overlying river water and hyporheic pore

115 water were collected using CTD Divers (van Essen Instruments, The Netherlands). The measurement cell of the CTD divers installed in the riverbeds were covered in nylon socks to prevent sediment from entering the measurement chamber of the logger which would interfere with EC measurements. In the present study, four pairs of EC time series were recorded in three urban rivers, which all receive considerable amounts of treated wastewater effluent.

Two time series were recorded in River Erpe at Heidemühle, Berlin (Germany, 52.478700°N, 13.635176°E). Previously

120 investigations at the site included studies on the fate of trace organic compounds in hyporheic sediments (Posselt et al., 2018; Schaper et al., 2018) and on river-to-groundwater travel times (Schaper et al., 2022). The location is characterized by losing conditions, i.e., surface water is infiltrating into an alluvial aquifer and the sediments are sandy. The first eight-day long dataset at River Erpe was collected in April 2016 in 19 cm depth by placing the CTD Diver within a cylindrical tube (Figure 1b). Similar to Schaper et al. (2018), the rim of the tube was level with the sediment-water interface and the tube was installed to

125 create a near one-dimensional flow path. A second dataset was collected in River Erpe 8 cm depth in January 2019 (Figure 1a).

The River-Ammer site is upstream of the City of Tübingen (Germany, 48.520751°N, 9.019334°E) and is characterized by loamy to sandy sediments. In River Ammer, a CTD Diver was installed in 8 cm depth according to the scheme depicted in Figure 1a. Data was recorded for 3 weeks in December 2020 and January 2021. In the River Sturt (Warriparri), data was

130 collected in March and April 2017 at a site roughly 3 kilometers downstream of a municipal WWTP (Australia, 35.024957°S, 138.688016°E). The CTD Diver was installed in 9 cm depth in the HZ according to Figure 1a.

Hydrology and
Earth System
Sciences
Discussions

2.2 Model

2.2.1 Governing Equation

In the present study, we parameterize transport of the EC signal in the riverbed via the one-dimensional (1-D) advection-
135 dispersion equation (Genuchten and Alves, 1982). In order to compensate for drifts in EC measurement and for effects
introduced by reactions a time-dependent offset, $o(t)$ (µS cm⁻¹), is added:

$$\frac{\partial \sigma_{cons}}{\partial t} + v(t)\left(\frac{\partial \sigma_{cons}}{\partial z} - \alpha \frac{\partial^2 \sigma_{cons}}{\partial z^2}\right) = 0 \tag{1}$$

$$\sigma_{sim}(t) = \sigma_{cons}(t) + o(t) \tag{2}$$

in which α (m) is the longitudinal dispersivity, z (m) denotes the depth below the sediment-water interface, v (m/h) is the
porewater velocity and σ_{cons} and σ_{sim} (µS cm⁻¹) denotes the conservative EC signal and the EC signal accounting for the
offset, respectively. We are fully aware that flowpaths in dynamic hyporheic sediments can shift with time, and that the spatial
140 variability of hydraulic properties in conjunction with transverse mixing can lead to travel-time distributions that cannot fully
be described by the 1-D advection-dispersion equation. However, inferring the parameters for 3-D spatially variable flow fields
from the available data would be impossible. Thus, we use equation 1 only as a parameterization to obtain time-dependent
transfer functions, and we consider the coefficients determined upon calibration as apparent ones. In particular, the time-
variable velocity may in reality reflect effects of both changes in the true porewater velocities and shifts in travel paths.
145 Similar to previous studies (Schaper et al., 2019), equation 1 is solved in Python using central differentiation in space (Crank-
Nicolson) and implicit-Euler time integration. EC time series in the surface water were used as concentration at the upper
boundary condition, and EC time series measured in the sediment as data used for model calibration (compare section 2.4).
The domain was chosen considerably longer than the distance from the river to the measurement point to minimize the effects
of the outflow boundary condition, where we have set the diffusive flux to zero. Continuous time-series of $v(t)$ and $o(t)$ were
150 obtained by cubic-spline interpolation between a fixed number of distinct time points at regular intervals.

2.2.2 Regularized parameter inference

The time-invariant longitudinal dispersivity α and the n-tupels of the apparent porewater velocities (**v**) and the EC offset (**o**)
at distinct time points were adjusted during parameter inference. For the EC offset, the time resolution was set to one value
per 24 h for all model simulation conducted in the present study. The time resolution of the apparent porewater velocity was
155 altered during different model simulations. In the present study, four model scenarios (A-D) with different time resolution
were constructed: A with one velocity value per day, B with two apparent velocity values per day, C with four values per day,
and D with eight values per day, respectively. The prior distributions for α, **v** and **o** were set to be uniform with minimum and
maximum values of and 0.0001 m and 0.01 m, 0.0025 m h⁻¹ and 0.15 m h⁻¹ and -0.1 and 0.1 µS cm⁻¹, respectively.
Inference of model parameters (v, o, α) was achieved using the differential evolution adaptive metropolis algorithm DREAM
160 of Vrugt (2016). DREAM uses multiple Markov chains, subspace sampling, outlier detection and a Metropolis-Hasting

sampling to derive posterior probability parameter distributions (posteriors) of the model parameters. Twenty-eight Markov chains were run in parallel during each DREAM simulation. The posterior distribution was sampled during 14,000 iterations performed after the Markov chains had converged, which was defined by the $\hat{R}$-statistic of Gelman and Rubin (1992) for each model parameter to be smaller than 1.2.

165 Assuming a constant measurement error SD_{obs} (μS cm^{-1}) of EC, the log-likelihood of the measurements can be written as:

$$\mathcal{L}(\boldsymbol{\sigma}_{meas}|SD_{obs},\boldsymbol{v},\boldsymbol{o},\alpha) = -\frac{1}{2}\sum_{t=1}^{m}\left[\left(\frac{\sigma_{meas,t} - \sigma_{sim,t}(\boldsymbol{v},\boldsymbol{o},\alpha)}{SD_{obs}}\right)^2\right] \quad (3)$$

subject to a constant that does not depend on the parameters. Here $\boldsymbol{\sigma}_{meas}$ denotes the vector of all EC-measurements, and $\sigma_{sim,t}(\boldsymbol{v},\boldsymbol{o},\alpha)$ is the simulated EC value at the measurement time with index t (-). To penalize large fluctuations in the porewater velocity $v(t)$ and the EC offset $o(t)$, the sum of squared differences between two subsequent parameter estimates, multiplied by regularization weights w_v (h^2 m^{-2}) for porewater velocity and w_o (cm^2 μS^{-2}] for EC offset, were added to the

170 log-likelihood function to construct the posterior log-likelihood $\mathcal{L}_a$ of the parameters $\boldsymbol{v},\boldsymbol{o},\alpha$, given the measurements $\boldsymbol{\sigma}_{meas}$ and the model:

$$\mathcal{L}_a(\boldsymbol{v},\boldsymbol{o},\alpha|\boldsymbol{\sigma}_{meas})$$

$$= -\frac{1}{2}\sum_{t=1}^{m}\left[\left(\frac{\sigma_{meas,t} - \sigma_{sim,t}(\boldsymbol{v},\boldsymbol{o},\alpha)}{SD_{obs}}\right)^2\right] - w_v\sum_{j=1}^{n_v-1}\left(v_{j+1} - v_j\right)^2$$

$$- w_o\sum_{j=1}^{n_o-1}\left(o_{j+1} - o_j\right)^2 \quad (4)$$

in which n_v (-) and n_o (-) are the numbers of velocity and offset values, respectively, subject to a constant that does not depend on the parameters.

The optimal regularization weights w_v and w_o were found by the L-curve method (Hansen and O'Leary, 1993), i.e., by plotting

175 the squared Euclidian norm of the residuals $\left(\sum_{t=1}^{m}\left[\left(\sigma_{meas,t} - \sigma_{sim,t}(\boldsymbol{v},\boldsymbol{o},\alpha)\right)^2\right]\right)$ versus the squared Euclidian norm of the consecutive difference of parameter values $\left(\sum_{j=1}^{j-1}\left(x_{j+1} - x_j\right)^2\right)$ for different values of w_v and w_o. Weights were considered optimal along the L-curve where its curvature was the highest. Here, additional smoothing would incur relatively large deterioration of the model fit, whereas less smoothing would lead to unnecessary parameter fluctuations. The optimal weights were located by visual inspection of the L-curve and assigned to pairs of w_v and w_o. For all model runs, the root-mean square

180 error (RMSE) was calculated as an additional measure of the goodness of fit between the measured EC signal and the EC signal simulated using the best performing parameter set of each run.

Hydrology and
Earth System
Sciences
Discussions

Open Access

EGU

2.2.3 Calculation of time-dependent advective travel time

The time-dependent advective travel time from the surface water to a location in the streambed sediment was calculated from the time-dependent apparent porewater velocity in two steps. First, the cumulative distance, $d(t)$, covered by a water parcel along a hypothetical flow line was calculated as a function of time t:

$$d(t) = \int_o^t v(t_*)dt_*$$

(5)

With $v(t_*) > 0 \; \forall t_*$ the cumulative-distance function $d(t)$ is monotonic. The advective age $\tau(t)$ at the observation point at time t is then defined by the following root-finding problem:

$$d(t) - d\big(t - \tau(t)\big) - \Delta z = 0$$

(6)

where Δz is the measurement depth.

2.2.4 Non-parametric deconvolution

The method of non-parametric deconvolution assumes linear and time-invariant transport. Then, any output signal $y(t)$ can be calculated by convoluting the transfer function $g(\tau)$ and the input signal $x(t)$ (Jury, 1982):

$$y(t) = \int_0^T g(\tau)x(t - \tau)d\tau$$

(7)

In hydrological terms, the transfer function $g(\tau)$, also denoted as Green's function or impulse-response function, describes the linear response of the system to a pulse-like input function under stationary conditions. For solute transport, it can be interpreted as a travel-time distribution times the signal recovery. In deconvolution, $g(\tau)$ is inferred from measured $x(t)$ and $y(t)$ signals. In non-parametric deconvolution, the shape of the transfer function is not prescribed a priori, but is estimated from the measured data under the restriction that $g(\tau)$ is smooth and non-negative (Cirpka et al., 2007; Fienen et al., 2006). In the present study, transfer functions were estimated by the approach of Cirpka et al. (2007), which minimizes the following objective function (Vogt et al., 2010):

$$W = \frac{1}{\sigma_{ep}^2} \int_{\tau_{max}}^{t_{max}} \left(EC_{sed}(t) - \int_0^{\tau_{max}} g(\tau)EC_{riv}(t - \tau)d\tau \right)^2 dt + \frac{1}{2\theta} \int_0^{\tau_{max}} \left(\frac{\partial g}{\partial \tau} \right)^2 d\tau$$

(8)

subject to: $g(\tau) \geq 0 \; \forall \tau$

(9)

where $EC_{riv}(t)$ and $EC_{sed}(t)$ [μS cm⁻¹] are the deviations of the EC time-series in the river and its riverbed sediments from their respective mean values, τ_{max} [h] is the maximum time-offset considered in convolution, t_{max} [h] is the maximum time of the EC time series, σ_{ep} [μS cm⁻¹] is the homoscedastic epistemic model error, θ [d⁻³] can be interpreted as the slope of the linear semivariogram expressing the autocorrelation of $g(\tau)$. The values of the transfer function $g(\tau)$ and of the structural parameters σ_{ep} and θ are estimated iteratively by constrained maximum-likelihood estimation and the Expectation-

Maximization approach (McLachlan and Krishnan, 2007), respectively. Details of the method have been described by Cirpka

205   et al. (2007).

3 Results and Discussion

3.1 Dynamics of electrical conductivity and groundwater-surface water interactions

Time series of electrical conductivity (EC) measured in the surface water at the three study sites show pronounced and quasi-

210   periodic fluctuations that, together with diurnal temperature signals, propagated into streambed sediments (Figure 2b, Figures SI-06 to SI-09). In River Erpe and in Sturt River, EC fluctuations are characterized by a periodicity of approximately 24 h. EC time series in River Erpe are in line with diurnal temperature and stream stage fluctuations (Figure SI-06 & SI-07), which are caused by time-varying discharge of the large municipal wastewater treatment plant Münchehofe located approximately 0.8 km upstream of the study site (Jaeger et al., 2019). At the site, further research on river-to-groundwater travel times conducted

215   in June 2019 (Schaper et al., 2022) showed that stream stage variations resulted in diurnal pressure-head fluctuations in the adjacent riparian aquifer (recorded approximately 3 m away from River Erpe, Figure SI-04).

In River Ammer, EC fluctuations occur with a periodicity of approximately 8 h. They are caused by the quasi-periodic release of effluents from a drinking-water softening plant into River Ammer upstream of the sampling site (Schwientek et al., 2013). In the Sturt River, diurnal EC fluctuations were already present approximately 100 m downstream of the WWTP effluent

220   discharge point (Figure SI-05). They were likely amplified along the 3 km river reach upstream of the study site by mixing with tributaries in-stream processes such as stream metabolism and mixing. At the River-Ammer and Sturt-River field sites, levels of riparian groundwater were not recorded and thus, information on differences between stream stages and riparian groundwater levels is not available. Due to the propagation of EC signals from the surface water into hyporheic sediments at all field sites, however, it is reasonable to assume that the hyporheic flow paths sampled as part of the present study originated

225   in the rivers and that mixing with old groundwater can be neglected at all sites.

3.2 Model performance and effects of parameter regularization

For all four datasets, measured EC time series were better met with a higher temporal resolution of the apparent porewater velocity, by introducing a time-dependent EC offset ($log_{10}w_o$), and with low regularization weights (Figure 3). For the two highest temporal resolutions of apparent porewater velocities (i.e., 8 and 4 values per day, respectively), pairs of optimal

230   weighting factors for the EC offset ($log_{10}w_o$) and for porewater velocity ($log_{10}w_v$), determined by visual inspection of the L-curves, were 5 for the River Ammer and River Erpe 2019 datasets and 4 for the River Erpe 2016 and River Sturt datasets, respectively (Figure 3, Figures SI-01 to SI-03). For the River Erpe 2016 and River Ammer datasets an increase in temporal resolution from 4 to 8 velocity values per day resulted in a considerable improvement of the model fit, i.e., the mean RMSE (± two standard deviations) of all model realizations computed during posterior sampling decreased from $3.2 \pm 0.2 \, \mu S \, cm^{-1}$ to

Hydrology and
Earth System
Sciences
Discussions
Open Access
EGU

235   2.4 ± 0.2 µS cm^{-1} and from 7.1 ± 0.1 µS cm^{-1} to 6.1 ± 0.1 µS cm^{-1}, respectively (Table SI-01). For the River Erpe 2019 and

River Sturt datasets, however, improvements of the goodness of model fits were less pronounced when the temporal resolution

of apparent porewater velocities was increased from 4 to 8 values per day. The mean RMSE of all model realizations computed

during posterior sampling for 4 to 8 values per day were 2.6 ± 0.2 µS cm^{-1} and 2.5 ± 0.2 µS cm^{-1} for the River Erpe 2019 and

1.8 ± 0.1 µS cm^{-1} and 1.6 ± 0.1 µS cm^{-1} for the River Sturt dataset, respectively (Table SI-01).

240   The temporal resolution of apparent porewater velocity values is restricted by the mean travel time from the surface water to

the measurement location and the amplitude and the frequency of traceable features in the input and output signals. In the

River Ammer dataset, an improvement of model fit with an increase in temporal resolution from 4 to 8 velocity values per

day, is likely related to higher-frequency periodicity of EC surface water fluctuations compared to the Sturt River and River

Erpe datasets. However, whether the improvement of model fit with an increase in temporal resolution from 4 to 8 velocity

245   values per day observed in the River Erpe 2016 dataset, but not the Sturt River and River Erpe 2019 datasets, is related to input

time series characteristics (e.g., higher amplitudes of higher order harmonics) or flow-path characteristics, remains unclear. In

the subsequent sections, model parameters are reported and discussed for the model scenarios with the highest temporal

resolution of apparent porewater velocities and optimal weighting factors only.

3.3 Estimated model parameters and temporal dynamics of porewater velocities

250   For the highest temporal resolution of porewater velocities and optimal weighting factors, median (± 1 interquartile range IQR)

apparent porewater velocity calculated from the posterior probability density distributions (posteriors) of all but the first

estimated value ranged between 1.1 ± 1.6 cm h^{-1} for River Ammer to 2.8 ± 0.5 for River Sturt, respectively, while the median

(± 1 IQR) of the EC offset ranged between -26 ± 8 µS cm^{-1} for River Ammer to 56 ± 10 µS cm^{-1} for River Erpe 2019 (Table

1). For the same model scenarios, mean (± 2 SD) longitudinal dispersivity values ranged between 1.3 ± 0.4 cm in the River

255   Sturt dataset to 8.9 ± 0.4 cm in the River Ammer dataset (Table 1). Different temporal resolutions of apparent porewater

velocities had only little effect on their overall temporal mean, longitudinal dispersivity, and EC offset values (Table SI-01).

The conditional mean time series of apparent porewater velocity and EC offset, calculated for the highest temporal resolution

of porewater velocity and optimal weighting factors, showed pronounced temporal variability in all datasets (Figure 2, Figures

SI-06 to SI-09, Figure SI-14). Mean ± 1 SD (maximum) diurnal relative porewater velocity changes (in % $v_{min}v_{max}^{-1}$) ranged

260   between 34 ± 15 (17) % in the Sturt River time series to 82 ± 10 (68) % in the River Erpe 2019 time series, respectively (Table

1).

Longitudinal dispersivity (α_L) is a function of sediment heterogeneity and grain size distribution and differences observed

between the datasets analyzed in the present study are likely related to sediment properties of the respective sampling sites.

The mean values estimated from the four datasets evaluated in the present study are in line with values estimated by a laboratory

265   (Chou and Wyseure, 2009) and a field study (Liu et al., 2019) where α_L was found to be in the order of several centimeters.

Reactive processes in the hyporheic zone alter overall EC of the porewater. First of all, water-rock interactions and precipitation

reactions might cause changes of the EC offset. Redox processes in the hyporheic zone might also alter the EC offset. The EC

offset values could be subject to diurnal variations because of diurnal variations of the CO_2 partial pressure in the infiltrating

water (via photosynthesis) and of diurnal temperature fluctuations. In addition, EC measurement devices including the CTD

270   divers used here can be subject to drift. The estimated best-fitting time series of the EC offset did not correlate to the measured

temperature in the streambed sediment (i.e., Spearman $\rho < 0.3$), neither to the estimated time series of apparent porewater

velocity nor to the measured EC values in both the surface and porewater (Figures SI-10 to Figures SI-13). An exception was

found for the Sturt River dataset in which the EC offset correlated positively with the measured EC in both porewater and

surface water (i.e., Spearman rank correlation coefficient > 0.6, p-value < 0.01, Figure SI-13). It is thus likely, that the temporal

275   dynamics of EC offset are predominantly related to measurement error, although effects of biogeochemical processes in

streambed sediments cannot be fully excluded without detailed knowledge on surface water and porewater ion composition.

In the approach outlined in section 2.2, the EC signal measured in the HZ is treated as a point measurement, although the EC

measurement in the CTD Divers used in the present study is performed in a cell with an inner diameter of approximately 1 cm.

The uncertainty ranges reported above should thus be viewed as model uncertainties that incorporate EC signal measurement

280   uncertainty but do not incorporate conceptual errors arising from the fact that EC measurements were not truly performed as

point measurements and that the installed CTD divers may have influenced local flow fields.

Estimates of apparent porewater velocity in the present study generally fall within the range of values found in streambed

sediments in a variety of rivers which can range from a few cm per day up to a meter per hour (Boano et al., 2014). For the

two datasets collected in River Erpe, the estimated porewater velocities compared well to previous studies at the same site, in

285   which vertical velocities were estimated from EC and temperature time series resulting in values in the order of several cm per

hour (Schaper et al., 2018, 2019).

Water exchange flows across the sediment water interface are driven by head gradients, typically occur over geomorphological

features of various spatial scales ranging from streambed ripples and dunes to pool-riffle sequences and meanders and can be

strongly influenced by riparian and regional groundwater levels (e.g., Krause et al., 2022). In the River Erpe 2016 dataset,

290   apparent porewater velocity correlated positively with stream stage (Spearman $\rho = 0.73$, p < 0.01, Table 1), while in the River

Erpe 2019 dataset correlation between apparent porewater velocity and stream stage were less pronounced (Spearman $\rho =$

0.20, p < 0.01), although mean ($\pm$ 1 SD) diurnal stream stage ranges were only slightly smaller in the River Erpe 2019 (17 $\pm$ 4

cm) compared to the River Erpe 2016 modeling period (23 $\pm$ 1 cm). Because stream stage variations at the field site translate

to variations in pressure gradients between the river water stage and the riparian groundwater (section 3.1, Figure SI-04), it is

295   likely that flux transients in the River Erpe 2016 dataset are induced by diurnal variations of hydraulic gradients. However, at

the River Erpe site, diurnal hydraulic gradients seem only to result in diurnal porewater velocity fluctuations, if the flow field

is constrained to near one-dimensional flow conditions by a cylindrical tube. Stream stage and apparent porewater velocity

time series in the Sturt River and River Ammer datasets were also characterized by diurnal fluctuations, but in both datasets,

the time series did not correlate with each other. In River Ammer, the Sturt River and the River Erpe 2019 datasets, it is thus

300   likely that the flow field in the HZ was multidimensional and that flux transients in the hyporheic zone were related to spatial

shifts of flow paths over time rather than due to hydraulic-gradient variations along a fixed flow path. The fitted porewater

velocity time series thus incorporates not only true temporal variations of porewater velocity along a fixed flow path, but also other effects such as a shift in the spatial arrangement of flow paths and concurrent shifts in flow path lengths.

3.4 Dynamic travel times

305 The median advective travel time (median $\bar{\tau}_{ADE}$ ($\pm$ IQR)), estimated using the ADE model (sections 2.2 and 2.4) and calculated from all posterior model realizations (n = 1200) over all model timesteps ranged from 2.8 $\pm$ 1.0 h in the River-Erpe-2019 dataset to 7.0 $\pm$ 2.3 h in the River-Erpe-2016 dataset (Table 1). The normalized first raw moment ($\pm$ second central normalized moment) of the conditional mean of the stationary travel time distribution (TTD) estimated by non-parametric deconvolution (section 2.5) ranged from 3.3 $\pm$ 3.7 h for the River-Erpe-2019 dataset to 15.9 $\pm$ 10.9 h for the Sturt-River dataset. For the River-

310 Erpe-2019 and the River-Ammer datasets, median and IQR $\bar{\tau}_{ADE}$ thus compare well to the first raw and the second central moment of the estimated stationary residence time distribution, respectively. For the River-Erpe-2016 and the Sturt-River datasets, however, the first raw and the second central moments of the stationary TTDs overestimate the ADE derived median and IQR values. The TTD estimated from the River-Erpe-2019 dataset was found to be unimodal, the TTDs derived from the Erpe-2016 and River-Ammer datasets has one pronounced primary peak, which is followed by minor secondary peaks at

315 slightly higher residence times compared to the mode of the distribution and the TTD of Sturt River datasets is bimodal (Figure 4). Non-parametric deconvolution assumes that transport conditions are linear and time-invariant, but estimates TTDs without pre-defining a certain TTD shape. For the River-Erpe and River-Ammer datasets, TTDs in principle resemble inverse Gaussian distributions, suggesting that transport along the sampled flow paths is likely to be Fickian in nature (Simmons, 1982). Multimodality and broad peaks in travel-time distributions in saturated porous media have been considered to be the result of

320 mixing between distinct flow paths which may occur in highly heterogenous or layered aquifers (McCallum et al., 2014; Leray et al., 2016).

The approach presented in section 2.3 demonstrates that for three out of four datasets analyzed in the present study, solute transport in streambed sediments is highly time-dependent (section 3.3). Moreover, the 2016 dataset was collected within a cylindrical tube and thus flow conditions around the CTD diver were most likely one-dimensional. Multi- and bimodality in

325 deconvolution-derived TTDs is most pronounced in data sets with high temporal variability of the porewater velocity. Assuming that riverbed sediment heterogeneity across the sampled flow paths had little effects on the TTD shape, it is therefore likely that the multimodality, particularly in case of the River-Erpe-2016 dataset, is caused by flux transients. It should be noted, however, that the bimodal TTD estimated from the Sturt dataset, could also be a modeling artefact, which arose due to the inability of non-parametric deconvolution to correctly align the phase of the two semi-sinusoidal EC signals with a period

330 of 24 h.

4 Conclusion

Time series of electrical conductivity are an easy-to-measure, cost effective natural tracer to investigate transport in shallow (< 20 cm) streambed sediments under loosing conditions. In the present study, we estimated temporal dynamics of apparent porewater velocity in streambed sediments using a user-defined temporal resolution. However, a high temporal resolution of apparent porewater velocity requires regularization, which increases the computational costs and adds another step in the data analysis workflow. Our results demonstrate that diurnal stream stage variations can translate to substantial flux transients in riverbed sediments, with apparent porewater velocity changing considerably within a day (in our case by a factor of 6 within 24 h). The fitted flux transients may either be due to actual variations of porewater velocity along fixed flow paths induced by diurnal head gradient fluctuations or due to a shift of the spatial arrangement of flow paths and their lengths. Future studies that seek to quantitatively investigate reactive transport and biogeochemical processes in hyporheic sediments should thus consider porewater velocity as transient in their conceptual transport models, especially if the time scales of water sampling are in the order of hours or days.

The present study further shows that transport in shallow hyporheic zones is in many cases of a Fickian nature, indicating that ADE-based modelling approaches provide meaningful transport parameter estimates. However, flux transients can cause multimodality in non-parametric deconvolution-derived travel time distributions (TTDs). Estimation of transport characteristics (i.e., statistical moments) from travel time distributions derived from time series of electrical conductivity in riverbed sediments should be treated with caution, especially if the estimated TTDs contain tailings and multiple secondary peaks.

All four datasets evaluated in the present study were collected in rivers receiving water from urban water management facilities at time-variable rates, which was a major driver for the more or less periodic EC fluctuations encountered in their surface waters. Future studies should test the applicability of EC as a tracer in streambed sediments and the modeling approach presented in the present study also in rivers where EC fluctuations have less periodic causes (e.g., snowmelt and rainfall). A major drawback of EC as a natural tracer is that EC signals flatten out rapidly with increasing depth. Future research could seek to overcome this drawback by jointly inverting EC measurements and other natural tracers such as ^{222}Rn and heat.

Data availability

The data collected as part the present study are published as Schaper et al. (2023) and can be found at https://doi.org/10.5281/zenodo.7997796. The code of the model used in the present paper is available upon request from the corresponding author.

360 **Author contributions**

JLS wrote the manuscript, performed the data analysis and collected the data; OAC wrote sections of the manuscript, gave detailed comments and conceived of the model approach; JL gave comments and conceived of the sampling approach; CZ gave comments to the manuscript.

Competing interests

365 The authors declare that they have no conflict of interest.

References

Boano, F., Harvey, J. W., Marion, A., Packman, A. I., Revelli, R., Ridolfi, L., and Wörman, A.: Hyporheic flow and transport processes: Mechanisms, models, and bioghemical implications, Reviews of Geophysics, 52, 603–379,
375 https://doi.org/10.1002/2012RG000417.Received, 2014.

Chou, P. Y. and Wyseure, G.: Hydrodynamic dispersion characteristics of lateral inflow into a river tested by a laboratory model, Hydrol Earth Syst Sci, 12, 217–228, 2009.

Cirpka, O. A., Fienen, M. N., Hofer, M., Hoehn, E., Tessarini, A., Kipfer, R., and Kitanidis, P. K.: Analyzing bank filtration by deconvoluting time series of electric conductivity, Ground Water, 45, 318–328, https://doi.org/10.1111/j.1745-
380 6584.2006.00293.x, 2007.

Danckwerts, P. V.: Continuous flow systems. Distribution of residence times, Chem Eng Sci, 2, 1–13, https://doi.org/10.1016/0009-2509(96)81811-2, 1953.

Engdahl, N. B., McCallum, J. L., and Massoudieh, A.: Transient age distributions in subsurface hydrologic systems, J Hydrol (Amst), 543, 88–100, https://doi.org/10.1016/j.jhydrol.2016.04.066, 2016.

385 Fienen, M. N., Luo, J., and Kitanidis, P. K.: A Bayesian geostatistical transfer function approach to tracer test analysis, Water Resour Res, 42, 1–15, https://doi.org/10.1029/2005WR004576, 2006.

Frei, S. and Peiffer, S.: Exposure times rather than residence times control redox transformation efficiencies in riparian wetlands, J Hydrol (Amst), 543, 182–196, https://doi.org/10.1016/j.jhydrol.2016.02.001, 2016.

Gelman, A. and Rubin, D. B.: Inference from Iterative Simulation Using Multiple Sequences, Statistical Science, 7, 428–456,
390 https://doi.org/10.2307/2246134, 1992.

Genuchten, V. and Alves: Analytical solutions of the one-dimensional convenctive-dispersive solute transport equation, U.S. Deparment of Agriculture, Technical Bulletin, 1661, 151, 1982.

Ginn, T. R.: On the distribution of multicomponent mixtures over generalized exposure time in subsurface flow and reactive transport: Foundations, and formulations for groundwater age, chemical heterogeneity, and biodegradation, Water Resour Res,
395 35, 1395–1407, 1999.

Hansen, P. C. and O'Leary, D. P.: The use of the L-curve in the regularization of discrete ill-posed problems, SIAM journal on scientific computing, 14, 1487–1503, 1993.

Harvey, J. W., Böhlke, J. K., Voytek, M. A., Scott, D., and Tobias, C. R.: Hyporheic zone denitrification: Controls on effective reaction depth and contribution to whole-stream mass balance, Water Resour Res, 49, 6298–6316,
400 https://doi.org/10.1002/wrcr.20492, 2013.

Hatch, C. E., Fisher, A. T., Revenaugh, J. S., Constantz, J., and Ruehl, C.: Quantifying surface water-groundwater interactions using time series analysis of streambed thermal records: Method development, Water Resour Res, 42, 1–14, https://doi.org/10.1029/2005WR004787, 2006.

Hayashi, M., Vogt, T., Mächler, L., and Schirmer, M.: Diurnal fluctuations of electrical conductivity in a pre-alpine river:
405 Effects of photosynthesis and groundwater exchange, J Hydrol (Amst), 450–451, 93–104, https://doi.org/10.1016/j.jhydrol.2012.05.020, 2012.

Heberer, T.: Tracking persistent pharmaceutical residues from municipal sewage to drinking water, J Hydrol (Amst), 266, 175–189, 2002.

Höhne, A., Lewandowski, J., Schaper, J. L., and McCallum, J. L.: Determining hyporheic removal rates of trace organic
410 compounds using non-parametric conservative transport with multiple sorption models, Water Res, 206, https://doi.org/10.1016/j.watres.2021.117750, 2021.

Huntscha, S., Rodriguez Velosa, D. M., Schroth, M. H., and Hollender, J.: Degradation of polar organic micropollutants during riverbank filtration: Complementary results from spatiotemporal sampling and push-pull tests, Environ Sci Technol, 47, 11512–11521, https://doi.org/10.1021/es401802z, 2013.

415 Jaeger, A., Posselt, M., Betterle, A., Schaper, J., Mechelke, J., Coll, C., and Lewandowski, J.: Spatial and Temporal Variability in Attenuation of Polar Organic Micropollutants in an Urban Lowland Stream, Environ Sci Technol, 53, 2383–2395, https://doi.org/10.1021/acs.est.8b05488, 2019.

Jury, W. A.: Simulation of solute transport using a transfer function model, Water Resour Res, 18, 363–368, https://doi.org/10.1029/WR018i002p00363, 1982.

420   Keery, J., Binley, A., Crook, N., and Smith, J. W. N.: Temporal and spatial variability of groundwater-surface water fluxes: Development and application of an analytical method using temperature time series, J Hydrol (Amst), 336, 1–16, https://doi.org/10.1016/j.jhydrol.2006.12.003, 2007.

Knapp, J. L. A., González-Pinzón, R., Drummond, J. D., Larsen, L. G., Cirpka, Olaf. A., and Harvey, J. W.: Tracer-based characterization of hyporheic exchange and benthic biolayers in streams, Water Resour Res, 1575–1594,
425   https://doi.org/10.1002/ 2016WR019393, 2017.

Krause, S., Abbott, B. W., Baranov, V., Bernal, S., Blaen, P., Datry, T., Drummond, J., Fleckenstein, J. H., Velez, J. G., Hannah, D. M., Knapp, J. L. A., Kurz, M., Lewandowski, J., Martí, E., Mendoza-Lera, C., Milner, A., Packman, A., Pinay, G., Ward, A. S., and Zarnetzke, J. P.: Organizational Principles of Hyporheic Exchange Flow and Biogeochemical Cycling in River Networks Across Scales, Water Resour Res, 58, https://doi.org/10.1029/2021WR029771, 2022.

430   Leray, S., Engdahl, N. B., Massoudieh, A., Bresciani, E., and McCallum, J.: Residence time distributions for hydrologic systems: Mechanistic foundations and steady-state analytical solutions, J Hydrol (Amst), 543, 67–87, https://doi.org/10.1016/j.jhydrol.2016.01.068, 2016.

Lewandowski, J., Arnon, S., Banks, E., Batelaan, O., and Betterle, A.: Is the Hyporheic Zone Relevant beyond the Scientific Community ?, Water (Basel), 11, 1–33, https://doi.org/10.3390/w11112230, 2019.

435   Liu, D., Zhao, J., Jeon, W. H., and Lee, J. Y.: Solute dynamics across the stream-to-riparian continuum under different flood waves, Hydrol Process, 33, 2627–2641, https://doi.org/10.1002/hyp.13515, 2019.

Luo, J., Cirpka, O. A., Fienen, M. N., Wu, W. M., Mehlhorn, T. L., Carley, J., Jardine, P. M., Criddle, C. S., and Kitanidis, P. K.: A parametric transfer function methodology for analyzing reactive transport in nonuniform flow, J Contam Hydrol, 83, 27–41, https://doi.org/10.1016/j.jconhyd.2005.11.001, 2006.

440   Maloszewski, P. and Zuber, A.: Principles and practice of calibration and validation of mathematical models for the interpretation of environmental tracer data in aquifers, Adv Water Resour, 16, 173–190, https://doi.org/10.1016/0309-1708(93)90036-F, 1993.

McCallum, J. L., Engdahl, N. B., Ginn, T. R., and Cook, P. G.: Nonparametric estimation of groundwater residence time distributions: What can environmental tracer data tell us about groundwater residence time?, Water Resour Res, 50, 2022–
445   2038, https://doi.org/10.1002/2013WR014974, 2014.

McCallum, J. L., Cook, P. G., and Simmons, C. T.: Limitations of the Use of Environmental Tracers to Infer Groundwater Age, Groundwater, 53, 56–70, https://doi.org/10.1111/gwat.12237, 2015.

McLachlan, G. J. and Krishnan, T.: The EM Algorithm and Extensions, John Wiley, New York, 1–369 pp., https://doi.org/10.1002/9780470191613, 2007.

450   de Montety, V., Martin, J. B., Cohen, M. J., Foster, C., and Kurz, M. J.: Influence of diel biogeochemical cycles on carbonate equilibrium in a karst river, Chem Geol, 283, 31–43, https://doi.org/10.1016/j.chemgeo.2010.12.025, 2011.

Peralta-Maraver, I., Galloway, J., Posselt, M., Arnon, S., Reiss, J., Lewandowski, J., and Robertson, A. L.: Environmental filtering and community delineation in the streambed ecotone, Sci Rep, 8, 1–11, https://doi.org/10.1038/s41598-018-34206-z, 2018.

455   Pittroff, M., Frei, S., and Gilfedder, B. S.: Quantifying nitrate and oxygen reduction rates in the hyporheic zone using 222Rn to upscale biogeochemical turnover in rivers, Water Resour Res, 53, 563–579, https://doi.org/10.1111/j.1752-1688.1969.tb04897.x, 2017.

Posselt, M., Jaeger, A., Schaper, J. L., Radke, M., and Benskin, J. P.: Determination of polar organic micropollutants in surface and pore water by high-resolution sampling-direct injection-ultra high performance liquid chromatography-tandem mass
460   spectrometry, Environ Sci Process Impacts, 20, 1716–1727, https://doi.org/10.1039/c8em00390d, 2018.

Schaper, J. L., Seher, W., Nützmann, G., Putschew, A., Jekel, M., and Lewandowski, J.: The fate of polar trace organic compounds in the hyporheic zone, Water Res, 140, 158–166, https://doi.org/10.1016/j.watres.2018.04.040, 2018.

Schaper, J. L., Posselt, M., Bouchez, C., Jaeger, A., Nuetzmann, G., Putschew, A., Singer, G., and Lewandowski, J.: Fate of Trace Organic Compounds in the Hyporheic Zone: Influence of Retardation, the Benthic Biolayer, and Organic Carbon,
465   Environ Sci Technol, 53, 4224–4234, https://doi.org/10.1021/acs.est.8b06231, 2019.

Schaper, J. L., Zarfl, C., Meinikmann, K., Banks, E. W., Baron, S., Cirpka, O. A., and Lewandowski, J.: Spatial variability of radon production rates in an alluvial aquifer affects travel time estimates of groundwater originating from a losing stream, Water Resour Res, 1–22, https://doi.org/10.1029/2021wr030635, 2022.

Schmidt, C., Musolff, A., Trauth, N., Vieweg, M., and Fleckenstein, J. H.: Transient analysis of fluctuations of electrical
470   conductivity as tracer in the stream bed, Hydrol Earth Syst Sci, 16, 3689–3697, https://doi.org/10.5194/hess-16-3689-2012, 2012.

Schwientek, M., Osenbrück, K., and Fleischer, M.: Investigating hydrological drivers of nitrate export dynamics in two agricultural catchments in Germany using high-frequency data series, Environ Earth Sci, 69, 381–393, https://doi.org/10.1007/s12665-013-2322-2, 2013.

475   Sheets, R. A., Darner, R. A., and Whitteberry, B. L.: Lag times of bank filtration at a well field, Cincinnati, Ohio, USA, J Hydrol (Amst), 266, 162–174, https://doi.org/10.1016/S0022-1694(02)00164-6, 2002.

Simmons, C. S.: A stochastic-convective transport representation of dispersion in one-dimensional porous media systems, Water Resour Res, 18, 1193–1214, https://doi.org/10.1029/WR018i004p01193, 1982.

Stallman, R. W.: Steady one-dimensional fluid flow in a semi-infinite porous medium with sinusoidal surface temperature, J
480   Geophys Res, 70, 2821–2827, https://doi.org/10.1029/jz070i012p02821, 1965.

Tikhonov, A. and Arsenin, V. J.: Solutions of ill-posed problems, Halsted, New York, 1977.

Varni, M. and Carrera, J.: Simulation of groundwater age distributions, Water Resour Res, 34, 3271–3281, 1998.

Vieweg, M., Kurz, M. J., Trauth, N., Fleckenstein, J. H., Musolff, A., and Schmidt, C.: Estimatingtime-variable aerobic respiration in the streambed by combining electrical conductivity and dissolved oxygen time series, J Geophys Res Biogeosci,
485   121, 2199–2215, https://doi.org/10.1002/2016JG003345.Received, 2016.

Vogt, T., Hoehn, E., Schneider, P., Freund, A., Schirmer, M., and Cirpka, O. A.: Fluctuations of electrical conductivity as a natural tracer for bank filtration in a losing stream, Adv Water Resour, 33, 1296–1308, https://doi.org/10.1016/j.advwatres.2010.02.007, 2010.

490 Vrugt, J. A.: Markov chain Monte Carlo simulation using the DREAM software package: Theory, concepts, and MATLAB implementation, Environmental Modelling and Software, 75, 273–316, https://doi.org/10.1016/j.envsoft.2015.08.013, 2016.

Wu, L., Singh, T., Krause, S., Gomez-velez, J., Nützmann, G., and Lewandowski, J.: Impact of Dynamically Changing Discharge on Hyporheic Groundwater Conditions, 76–93, https://doi.org/10.1029/2018WR023185, 2018.

Wu, L., Gomez-velez, J. D., and Krause, S.: Impact of Flow Alteration and Temperature Variability on Hyporheic Exchange, https://doi.org/10.1029/2019WR026225, 2020.

495 Young, P. C., Pedregal, D. J., and Tych, W.: Dynamic harmonic regression, J Forecast, 18, 369–394, https://doi.org/10.1002/(SICI)1099-131X(199911)18:6<369::AID-FOR748>3.0.CO;2-K, 1999.

Zarnetske, J. P., Haggerty, R., Wondzell, S. M., and Baker, M. A.: Dynamics of nitrate production and removal as a function of residence time in the hyporheic zone, J Geophys Res Biogeosci, 116, 1–12, https://doi.org/10.1029/2010JG001356, 2011.

500
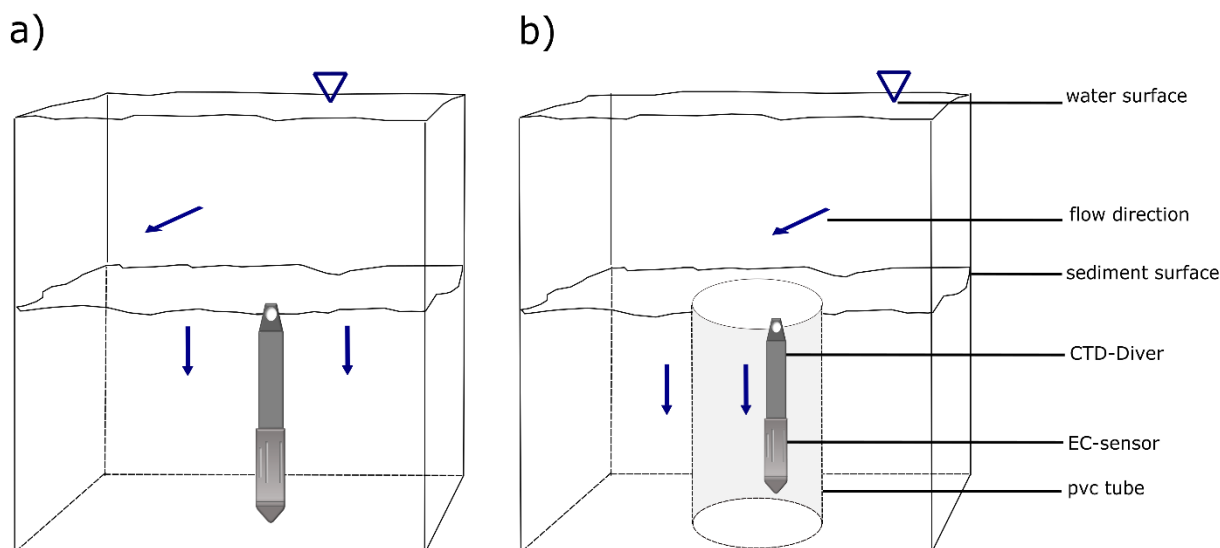
Figure 1 a) Placement of CTD divers within the riverbed sediments in River Ammer, the Sturt River, and in River Erpe in 2019. b) The River Erpe 2016 data set was recorded inside a 32 cm long ring enclosure (PVC pipe) to minimize the effects of horizontal flow components.
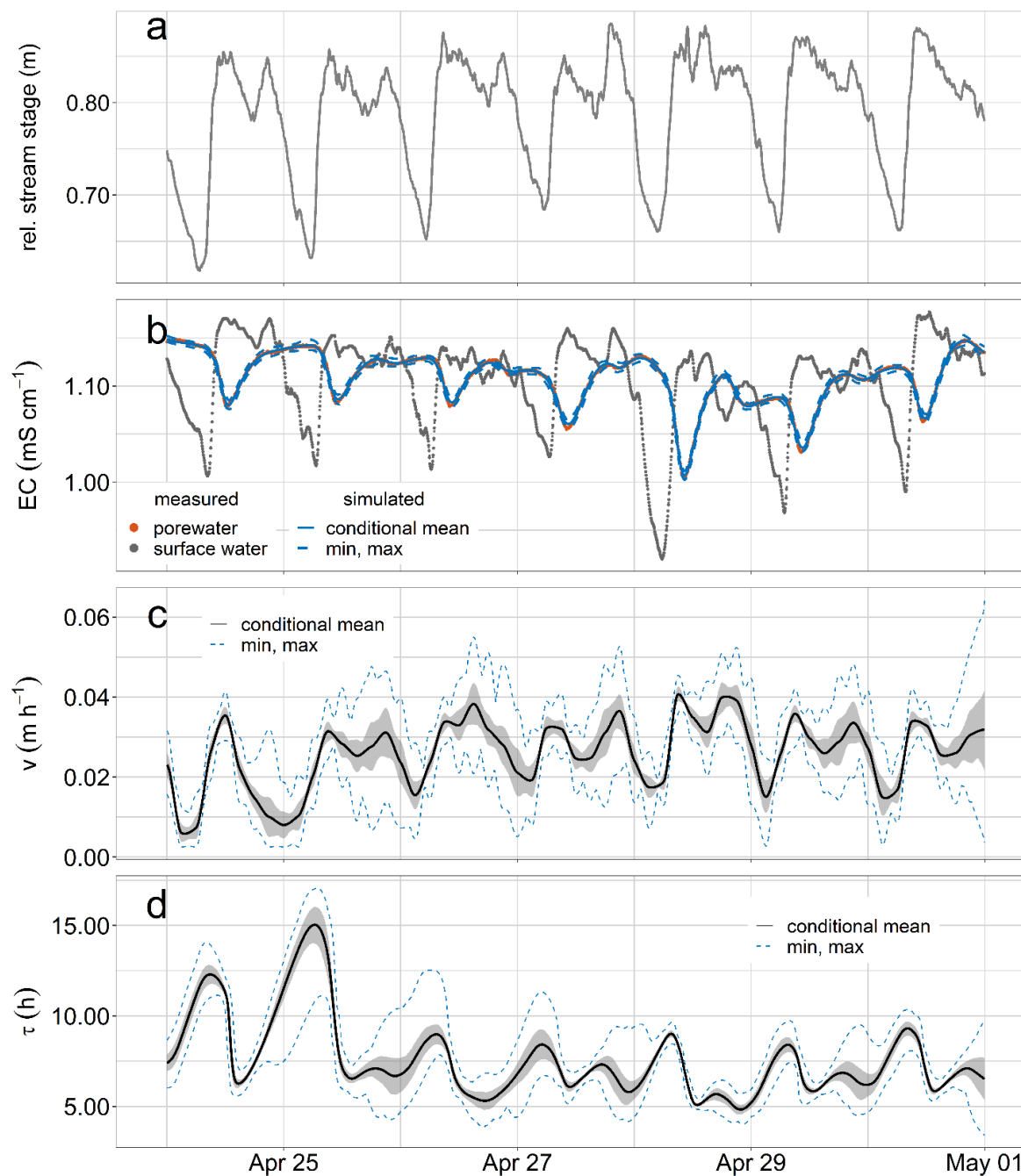
505

Figure 2 a) Stream stage variations relative to CTD diver installation depth in the surface water b) measured (dots) and modeled (lines) time series of electrical conductivity in River Erpe 2016 dataset c) measured and modeled time series of apparent porewater velocity v and d) mean advective travel time τ from surface water to the sediment depth of the logger. Grey areas denote one standard deviation around the conditional mean calculated from all accepted model realizations during posterior sampling.

510

18
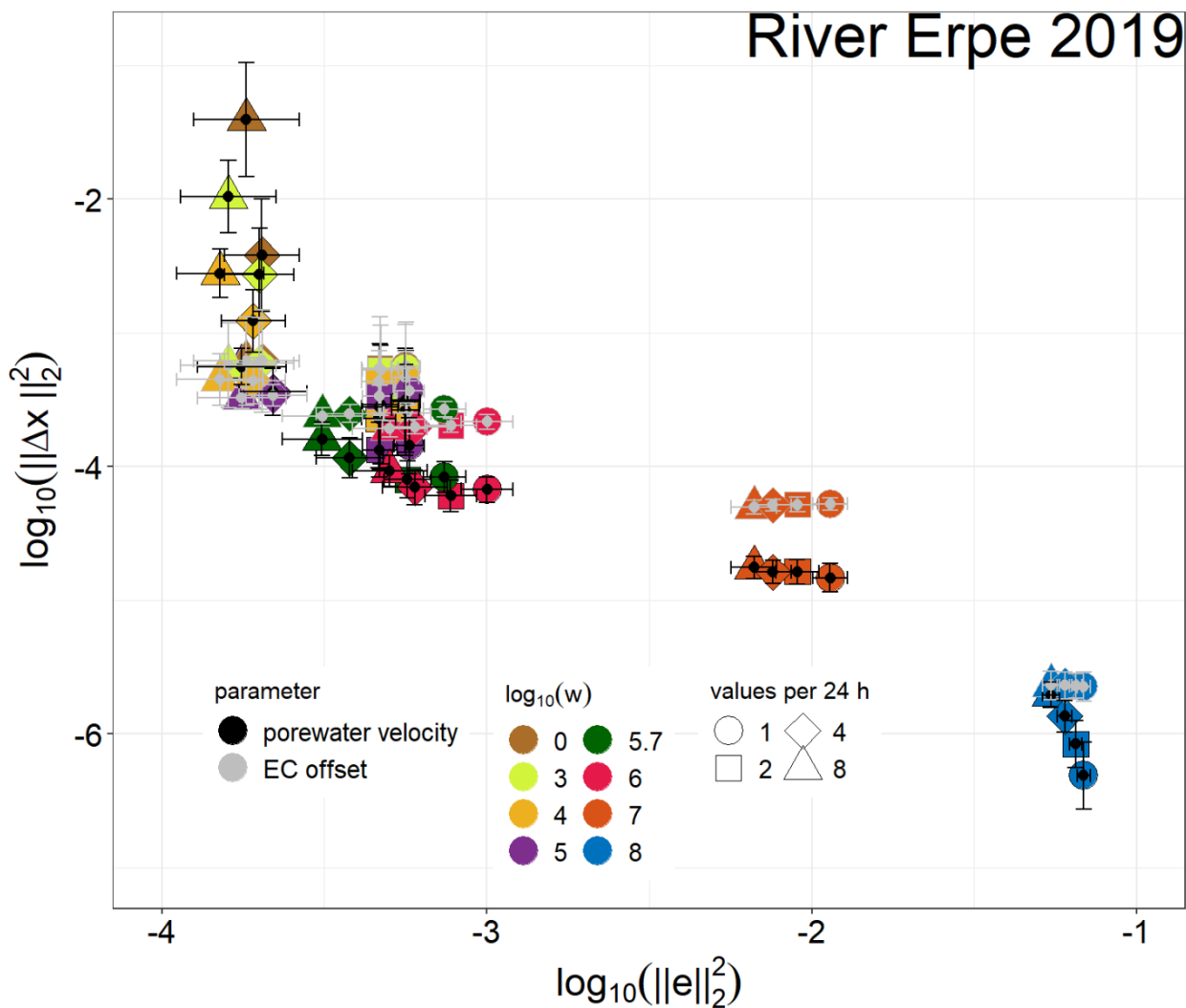
Figure 3 L-curve, i.e., a plot the decadic logarithm of the squared Euclidian norm of the model residuals, $log_{10}(\|e\|_2^2)$, versus the squared Euclidian norm of the consecutive difference of parameter values, $log_{10}(\|\Delta x\|_2^2)$, for all model runs conducted using the River Erpe 2019 dataset. The regularization weights w_v (h² m⁻²) for porewater velocity and w_o (cm² μS⁻²) for EC offset were varied (8 colors). For porewater velocity, one, two, four and eight staging posts d⁻¹ were used while the temporal resolution of the EC offset was one staging post per day. Weights are considered optimal along the L-curve where its curvature was the highest (i.e., $w_o = w_v = 1 \times 10^5$ for eight staging posts d⁻¹).
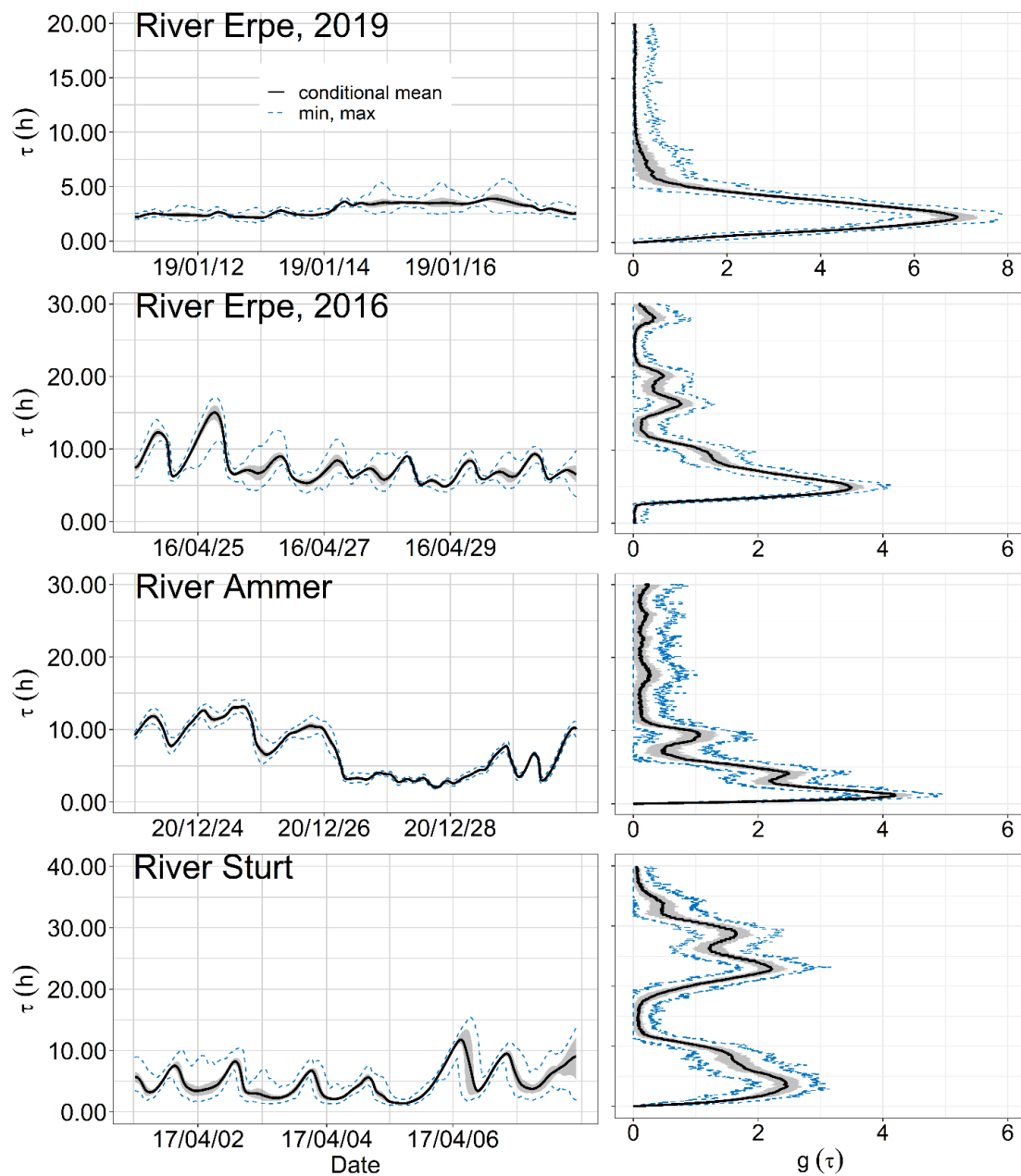
Figure 4 Time series of simulated mean advective travel time τ from surface water to the sediment depth of the logger calculated from estimated time-dependent velocities (left panels) and residence time distributions g(τ), estimated via non-parametric deconvolution (right panels), for the River Erpe, River Ammer and Sturt River datasets.

Table 1 Overview of dataset parameters (measurement depth and interval) and model settings, scenarios and results of both the advection-dispersion equation (ADE) based transport model and the non-parametric deconvolution approach. $\bar{\tau}_{ADE}$ = advective mean travel time; μ_τ = the mean travel time (i.e., the first raw moment normalized by the zeroth moment) of the travel time distribution (TTD) derived by non-parametric deconvolution; σ_τ = the variance of the travel time (i.e., the second central moment normalized by the zeroth moment) of the TTD.

		River Erpe, 2016	River Erpe, 2019	River Ammer	Sturt River
Measurement depth	cm	8	19	9	8
Measurement interval	min	5	5	2	2
ADE					
Number of apparent velocity values per day	d^{-1}	8	8	8	8
$\log_{10} w$	(-)	4	5	5	4
Mean $\alpha_L \pm 1$ SD α	cm	1.8 ± 0.1	1.0 ± 0.0	8.9 ± 0.2	1.5 ± 0.3
Median $v \pm$ IQR v	cm h^{-1}	2.7 ± 1.2	2.8 ± 1.0	1.1 ± 1.6	2.1 ± 2.1
Mean ± 1 SD $v_{min} v_{max}^{-1}$ (max.)	%	63 ± 13 (17)	82 ± 10 (68)	38 ± 14 (18)	34 ± 15 (17)
Median $\bar{\tau}_{ADE} \pm$ IQR	h	7.0 ± 2.3	2.8 ± 1.0	6.9 ± 6.6	4.2 ± 3.6
Spearman ρ: rel. Stream stage – cond. mean v	(-)	0.74	0.20	-0.59	-0.18
Deconvolution					
Epistemic error	mS cm^{-1}	0.025	0.013	0.025	0.0045
Slope of variogram θ	d^{-3}	1.6	10.96	11.55	2.00
Length of transfer function	n meas.	500	500	600	1300
$\mu_\tau \pm 1$ σ_τ	h	9.8 ± 7.2	3.3 ± 3.7	6.5 ± 7.4	15.9 ± 10.9